International Journal of Minerals, Metallurgy and Materials
Volume 19, Number 9, Sep 2012, Page 805
DOI: 10.1007/s12613-012-0632-0

Effects of precipitates and inclusions on the fracture toughness of hot rolling X70 pipeline steel plates

Mai-wen Zhou and Hao Yu

School of Materials Science and Engineering, University of Science and Technology Beijing, Beijing 100083, China
(Received: 10 October 2011; revised: 16 November 2011; accepted: 25 November 2011)

Abstract: In order to investigate the fracture toughness, crack tip opening displacement (CTOD) experiments were conducted on two X70 pipeline steel plates with different rolling processes. After the experiments, optical microscopy (OM), scanning electron microscopy (SEM) and transmission electron microscopy (TEM) were employed to observe the microstructure and fracture morphology. The effects of precipitates on the fracture toughness and the crack initiation mechanism induced by inclusions were analyzed. The CTOD result shows that the steel with a lower finishing cooling temperature has a higher fracture toughness. Inclusions with different shapes and two kinds of precipitates with different sizes were observed. It can be concluded that precipitates with different sizes have different effects and mechanisms on the fracture toughness. Distinguished from the earlier researches, inclusions enriched in silicon can be also served as the crack initiation.

Keywords: pipeline steel; crack propagation; precipitates; inclusions; fracture toughness

1. Introduction

In recent years, the development of high-strength pipeline steel technology has enabled the pipeline operators to realize significant cost saving [1-4]. As the pipe wall becomes thicker, more attentions are paid to the fracture toughness evaluation and improvement.

Material fracture resistance has historically been characterized as the absorbed energy or shear area by using Charpy V-notch or drop weight tear test (DWTT). However, with the development of high-grade pipelines and high-pressure rich gas transmission, the demand for the fracture toughness evaluation exceeds the current standard of the ductile fracture arrest evaluation model [5-6]. In this case new models based on the fracture mechanism are required. Featured by the application of full-thickness specimens and low loading rate which coincides with the practice, crack tip opening displacement (CTOD) is considered to be a true measurement of the ductile fracture resistance as well as a promising research direction [7]. Previous studies used CTOD only as a method to evaluate the fracture toughness around the weld seam [8]. However, based on the reasons mentioned above, it also has a wide application in the evaluation of the substrate toughness.

Precipitates and inclusions have significant influences on the fracture toughness. Precipitation strengthening is regarded as an effective strengthening way, and earlier researches mainly focus on their chemical compositions and sizes, but the systematic study of the strengthening mechanisms of precipitates with different sizes is rarely involved.

There exist several kinds of inclusions in the pipeline steel due to its complex alloy elements. The inclusions are mainly identified as aluminum oxide, calcium oxide/calcium sulfide, magnesium oxide, and manganese compounds [9]. The effect of inclusions on the crack initiation has not been fully understood because it depends on several factors, such as chemical composition, size, distribution, shape, adhesion of inclusions to the matrix, and the elastic constants of inclusions and the matrix [10].

In this work, CTOD experiment was conducted on two X70 steel plates with different rolling processes to investigate their fracture toughness. After the experiment, several methods were employed to observe the fracture morphology

Corresponding author: Mai-wen Zhou E-mail: zmwen1985@163.com

and the microstructure of the substrate. Moreover, the effects of inclusions were investigated, and the strengthening mechanisms of precipitates with different sizes were discussed systematically.

2. Experimental materials and procedures

2.1. Materials

Experimental pipeline steel plates used in this work were cut from two batches of hot rolling X70 plates with different chemical compositions and production process parameters. The differences are listed in Table 1 and Table 2 (provided by the manufacturer). In the factory inspection, steel A was judged to be unqualified for the low DWTT index.

2.2. CTOD experiments

The specimens were cut in accordance with the direction as shown in Fig. 1, and then machined to the final shape as shown in Fig. 2. The front of the fracture was marked to measure the fracture propagation distance. The multi-specimen method was adopted to determine the power-law fitting curve according to GB/T 21143—2007. The experimental temperature was −15°C and the whole test was conducted in Central Iron and Steel Research Institute Beijing.

Table 1. Chemical compositions of the two plates wt%

Steel	C	Si	Mn	P	S	Als	Alt	Nb	Ni	Mo	Ti
A	0.055	0.294	1.581	0.008	0.002	0.030	0.033	0.041	0.149	0.156	0.017
B	0.049	0.262	1.543	0.009	0.002	0.039	0.042	0.042	0.183	0.175	0.018

Table 2. Production process parameters of the two plates °C

Steel	SRT	FRT	SCT	FCT
A	937	830	790	594
B	934	834	796	500

Note: SRT—starting rolling temperature at the non-recrystallization region; FRT—finishing rolling temperature at the non-recrystallization region; SCT—starting cooling temperature; FCT—finishing cooling temperature.

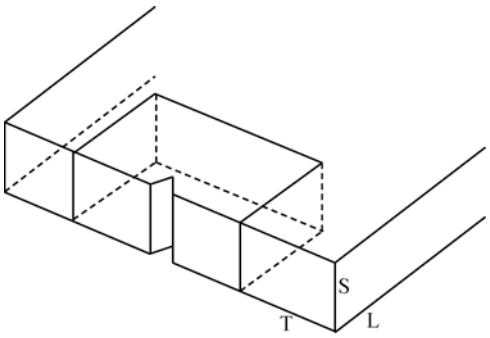

Fig. 1. Sampling direction of the CTOD experiment. T—transverse direction; S—short transverse direction; L—longitudinal direction.

2.3. Microstructure and morphology observation

The specimens at the quarter location along the thickness direction were polished and revealed by 4vol% nital solution. The microstructure was observed by using optical microscopy (OM), field emission scanning electron microscopy (FESEM) equipped with energy dispersive spectroscopy (EDS) and transmission electron microscopy (TEM). The fracture morphology was also examined by FESEM.

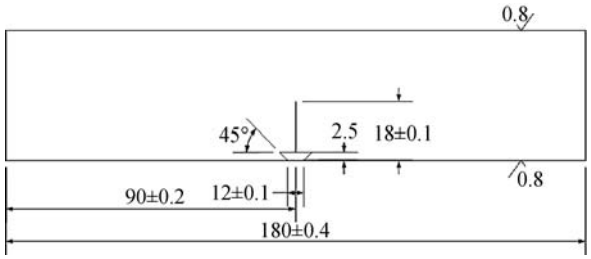

Fig. 2. Sample size of the CTOD experiment (unit: mm).

3. Results and analysis

3.1. CTOD result

The CTOD result of the two plates is shown in Fig. 3.

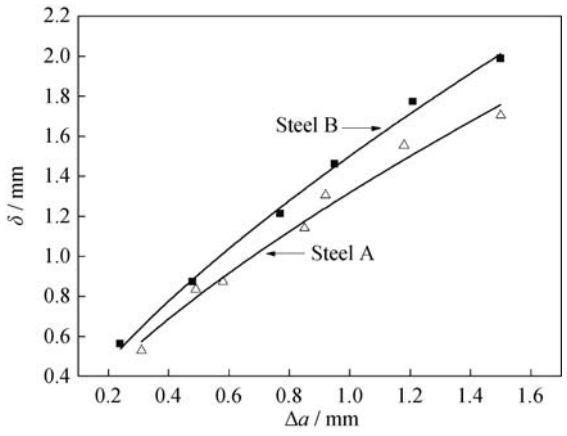

Fig. 3. Result of the CTOD experiment.

The power-law equations were fitted according to the experimental data. They are $\delta_1=1.4013\times\Delta a_1^{0.7736}$ and $\delta_2=1.296\times(0.1553+\Delta a_2)^{0.8978}$, respectively. The CTOD eigenvalues when Δa=0.05 mm and Δa=0.2 mm were calculated and listed in Table 3.

Table 3. CTOD eigenvalues of the two plates

Steel	$\delta_{0.05}$ / mm	$\delta_{0.2}$ / mm
A	0.162	0.241
B	0.313	0.512

The fracture toughness can be featured by the CTOD eigenvalues. The higher eigenvalues indicate the higher resistance against the fracture, that is, better fracture toughness, while the lower eigenvalues indicate the opposite. As shown in Table 3, the eigenvalues of steel B are twice as large as those of steel A, namely, steel B has a better fracture toughness than steel A. It can be also seen that the data points of steel A deviate the fitting curve more than steel B, which indicates the instability in fracture toughness of steel A.

3.2. Microstructure analysis

Fig. 4(a), 4(c), and 4(e) show the OM, SEM, and TEM images of steel A, respectively, while Fig. 4(b), 4(d), and 4(f) show the corresponding details of steel B. It can be seen from the OM image that steel A is composed of mostly granular bainite with little acicular ferrite. The bright punctate-distribution carbide can be observed in the SEM image.

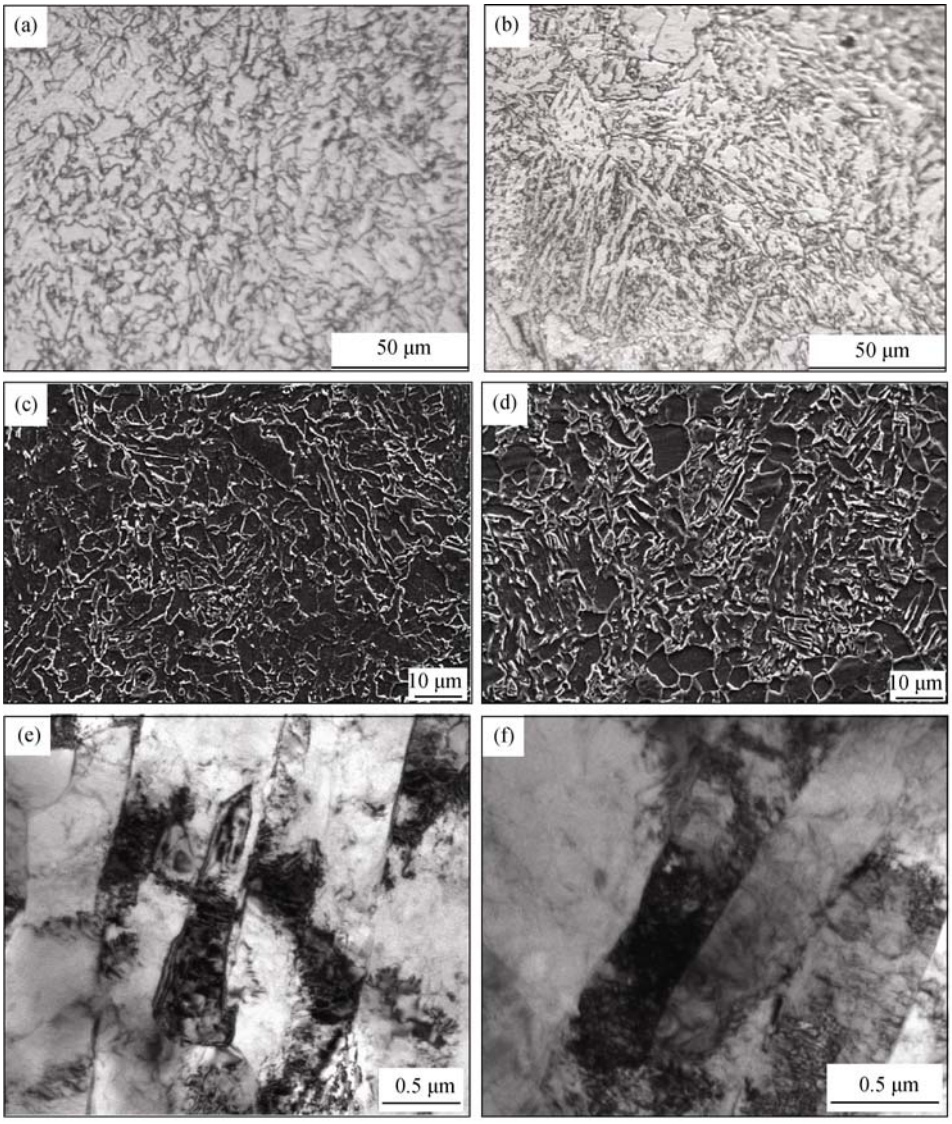

Fig. 4. Microstructures of the two plates: (a) OM image of steel A; (b) OM image of steel B; (c) SEM image of steel A; (d) SEM image of steel B; (e) TEM image of steel A; (f) TEM image of steel B.

Steel B contains large amounts of acicular ferrite with polygonal ferrite and granular bainite. The grain boundaries have different directions and are interlocked mutually with the M/A constituent distributed along and/or in them. The difference in microstructure may come from the different process parameters. When the final cooling temperature becomes high, the suppressed microstructure accounts for the majority due to the incomplete granular bainite transformation [11].

Typical lath morphology of the acicular ferrite can be found in steel B, in which exist a mass of dislocations. The same microstructure can be also observed in steel A, but the dislocation density is visually lower.

The characteristic of acicular ferrite with a small size, being interlocking-distributed, existing substructure and having high density of movable dislocations, ensures that the pipeline steel has good combination of high strength and toughness. This is an important reason why steel B has a better fracture toughness than steel A.

3.3. Fracture surface morphology

The crack initiation zone has ductile fracture because of low loading rate. Fig. 5 shows that the dimples of steel B are bigger in diameter and depth than those of steel A. The plasticity of materials and the strain-hardening exponent influence the mode that how microscopic voids cluster and cohere together. Materials with the high strain hardening exponent are generally difficult to generate necking down, so more microscopic voids will be connected by shear fracture. Therefore, the dimples become smaller and shallower.

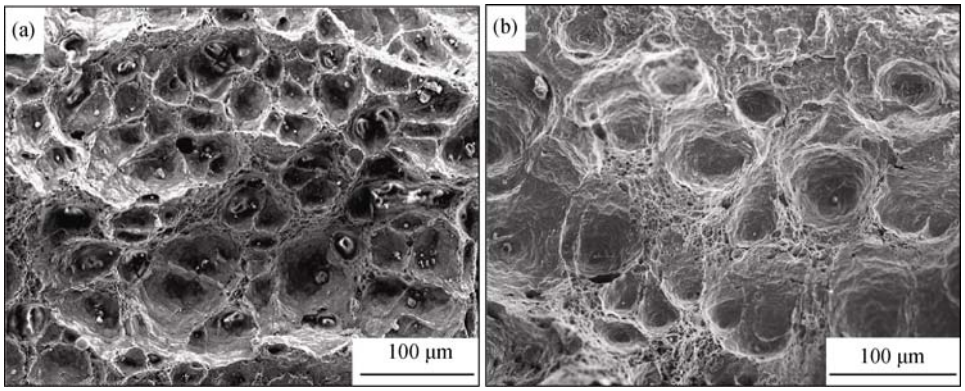

Fig. 5. SEM images of fracture morphology: (a) steel A; (b) steel B.

4. Discussion

4.1. Influence of inclusions on fracture toughness

4.1.1. Cubic inclusions

This kind of inclusions is mainly found around the dimples. Figs. 6(a) and 6(b) show that the cubic inclusions are mainly composed of Ti with little Nb, and the size is about 2 μm. According to the chemical composition and previous research [12], this kind of inclusions is TiN.

The solubility product of TiN is lower than that of TiC, NbN, and NbC, and their forming temperatures decrease successively; thus, TiN precipitates earlier than the others. Yu *et al.* [12] have reported that the carbide and nitride of Ti do not form in the liquid phase. TiN forms when the molten steel is solidified more than 40%, while TiC forms at the end of solidification. After this stage, they can dissolve each other to form a continuous solid solution—Ti(C,N), as TiN and TiC have the same crystallographic structure and approximate

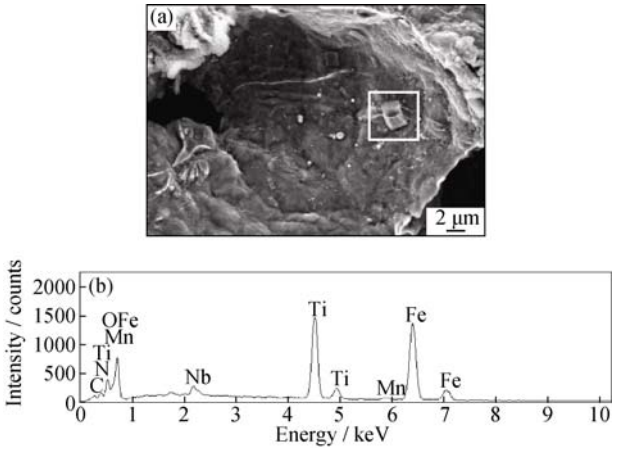

Fig. 6. SEM image (a) and EDS specturum (b) of cubic inclusions distributed in dimples.

lattice constant. During the following slow solidification and cooling stage, particles containing less Ti even Ti free (*e.g.* Nb(C,N)) precipitate on the existing TiN, which results in TiN growing up without changing the shape. Thus, particles

formed at a higher temperature have a large size (about 2 μm), enrich in Ti and appear to be square. In addition, these inclusions will not dissolve during soaking and hot rolling. As a result of large size, the pinning ability of such inclusions will be weak, and TiN cannot prevent the austenite grains from growing up effectively; therefore, the fracture toughness of the steel deteriorates.

4.1.2. Irregular inclusions

Irregular inclusions rarely distribute but often deteriorate the fracture toughness more. Even around the region far from the main fracture surface, the fracture can also initiate around the inclusions under the external force. Fig. 7(a) shows an inclusion of a comparatively large size, 20-40 μm approximately. Under low strain rate, the fracture has enough time to initiate around the inclusion, propagate, and connect with the main fracture surface.

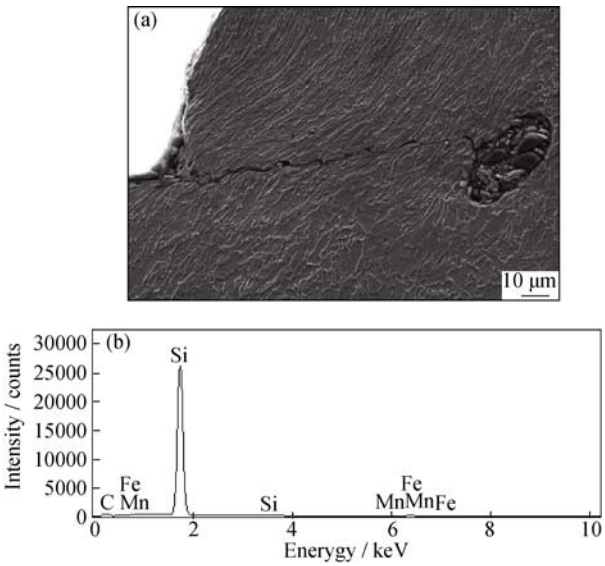

Fig. 7. SEM image of the fracture induced by irregular inclusions: (a) SEM image; (b) EDS spectrum.

Zhang [13] has pointed out that inclusions enriched in aluminum (*e.g.* Al_2O_3) are hard brittle as well as incoherent to the metal matrix. A quite big lattice deformation occurs nearby the inclusions. Consequently, microcracks and interstices are easily formed at the boundary between the inclusion and the metal. This theory has been widely accepted. Moreover, Liu *et al*. [14] claimed that inclusions enriched in Si were harmless to toughness because this kind of inclusions could be easily deformed, and there was a relatively small lattice deflection around such inclusions. However, the surface scan of this study (Fig. 8) shows that Si segregates at the fracture initiation zone.

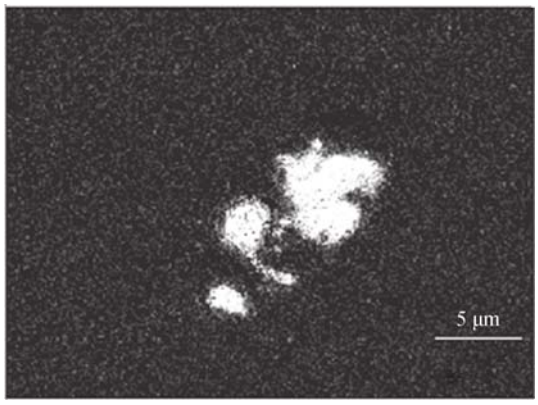

Fig. 8. Surface scan result of the irregular inclusion.

To interpret this phenomenon, it is necessary to analyze the formation mechanism of cracks induced by inclusions. Due to the weak interfacial bonding energy of inclusion/matrix, voids will form at very small strains around the inclusions [15]. At this time, the carbide/matrix interfaces are not yet broken. As the plastic strain increases, inclusion-induced voids grow as well. Under very large strains, these voids have grown very large in size, and at this time, many voids begin to initiate at carbides. The voids formed by carbides are small in size but large in quantity. They act as small cracks that distributed in the matrix among the large inclusion-induced voids. These small voids decrease the matrix's ability to bear the load. When the matrix can no longer bear the applied stress, voids begin to coalesce and ductile fracture occurs [16]. No definite evidence shows that alumina inclusions are the more preferential crack initiation sites than other inclusions [10]. From this point, we can conclude that, during the crack initiation, the size and the shape of the inclusion, as well as the gap between the inclusion and the matrix are more significant than the chemical composition of the inclusion.

4.2. Influence of precipitates on the fracture toughness

4.2.1. 200 nm scale precipitates

Fig. 9 shows a typical complex precipitate whose size is in the range of 100-200 nm. The EDS spectrum shows that it contains Ti and Nb (Fe and Mn mainly comes from the substrate). Dispersed in the matrix, these precipitates can reduce the austenite recrystallization temperature and restrain the austenite grains from growing up. As a consequence, fine acicular ferrite can be obtained by the thermomechanical control process (TMCP), and the high strength as well as toughness can be ensured. Wang *et al*. [17] reported that Nb-rich precipitates can nucleate in two ways: one is nucleation on the surface of the existing Ti-rich particles; the other is heterogeneous nucleation in the matrix

[18]. However, from the view of the free energy change theory, the former way is energetically preferred due to the remarkable decrease of the barrier energy for nucleation. Such a decrease comes from two parts: the absence of the requisite interfacial free energy needed for creating the precipitate/matrix interface and the strain energy used for the accommodation of the strain mismatch between the precipitate and matrix.

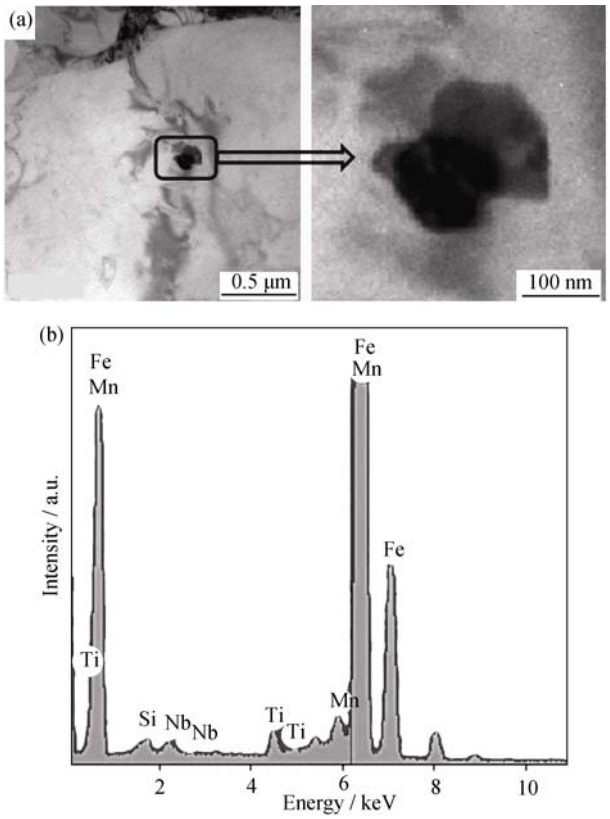

Fig. 9. Complex precipitate observed in steel A: (a) SEM image; (b) EDS spectrum.

4.2.2. 1-20 nm scale precipitates

Plenty of fine and dispersed precipitates distributed among the dislocation lines can be observed in Fig. 10. The precipitates of 1-20 nm have good pinning effect because they can prevent dislocations from moving or changing their motion paths. In addition, when suffering force, high density dislocation helps the crack tip emit more dislocations and form cellular structure, which is helpful to passivate the crack tip.

The precipitates of 200 nm and 1-20 nm both have positive effects on the fracture toughness, but they have different mechanisms. TiN cubes with a size of 200 nm precipitate in Ti- and N-enriched zones during solidification, so the particles are expected to be large. Such particles cannot pin dislocations effectively, but they can restrain grains from growing up, that is, they play a role in grain refinement strengthening. On the other hand, the particles of 1-20 nm, which precipitate after solidification, are expected to be relatively small, so they can serve the purpose as precipitation strengthening. According to Ref. [17], this kind of particles is observed both in the as-cast slab and in the hot band. As is well known, grain refinement strengthening and precipitation strengthening are the main strengthening ways in the pipeline steel.

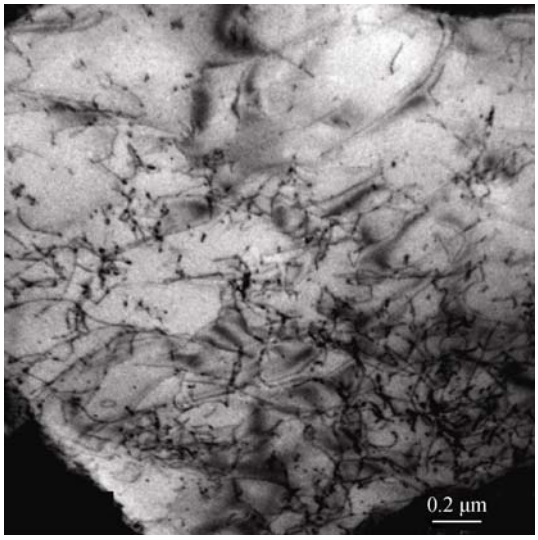

Fig. 10. TEM image of the fine precipitates observed in steel A.

5. Conclusions

(1) Steel A is composed of mostly granular bainite with little acicular ferrite, but steel B contains large amounts of acicular ferrite with polygonal ferrite and granular bainite. The main reason accounting for this difference is the higher final cooling temperature of steel A. Steel B has a better CTOD index coinciding with DWTT results in the factory inspection.

(2) Cubic TiN with a size of 2 μm mainly found around dimples cannot effectively prevent austenite grains from growing up.

(3) The behavior of cracks induced by inclusions is mainly determined by their area and the gap between the inclusion and the matrix. Inclusions enriched in Si can be also served as crack initiation.

(4) There are two types of precipitates distributing in the matrix. Relatively large precipitates have the effect of grain refinement strengthening on the steel, while fine precipitates have the effect of precipitation strengthening.

References

[1] B. Tanguy, T.T. Luu, G. Perrin, A. Pineau, and J. Besson, Plastic and damage behavior of a high strength X100 pipeline steel: experiments and modeling, *Int. J. Pressure Vessels Piping*, 85(2005), No.5, p.322.

[2] S.S. Nayak, R.D.K. Misra, J. Hartmann, F. Siciliano, and J.M. Gray, Microstructure and properties of low manganese and niobium containing HIC pipeline steel, *Mater. Sci. Eng. A*, 494(2008), p.456.

[3] K.T. Corbett, R.R. Bowen, and C.W. Petersen, High-strength steel pipeline economics, *Int. J. Offshore Polar Eng.*, 14(2004), p.75.

[4] H.B. Xue and Y.F. Cheng, Characterization of inclusions of X80 pipeline steel and its correlation with hydrogen-induced cracking, *Corros. Sci*., 53(2011), p.1201.

[5] D.J. Horsley, Background to the use of CTOA for prediction of dynamic ductile fracture arrest in pipelines, *Eng. Fract. Mech*., 70(2003), p.547.

[6] R. Ince, Determination of concrete fracture parameters based on two-parameter and size effect models using split-tension cubes, *Eng. Fract. Mech*., 77(2010), p.2233.

[7] M. He and F.G. Li, Modified transformation formulae between fracture toughness and CTOD of ductile metals considering pre-deformation effects, *Eng. Fract. Mech*., 77(2010), p.2763.

[8] A.S. Kumar, B.R. Kumar, G.L. Datta, and V.R. Ranganath, Effect of microstructure and grain size on the fracture toughness of a micro-alloyed steel, *Mater. Sci. Eng. A*, 527(2010), No.4-5, p.954.

[9] H.V. Atkinson and G. Shi, Characterization of inclusions in clean steels: a review including the statistics of extremes methods, *Prog. Mater. Sci.*, 48(2003), No.5, p.457.

[10] J. Ma, B. Zhang, D.K. Xu, E.H. Han, and W. Ke, Effects of inclusion and loading direction on the fatigue behavior of hot rolled low carbon steel, *Int. J. Fatigue*, 32(2010), p.1116.

[11] H. Yu, Influences of microstructure and texture on crack propagation path of X70 acicular ferrite pipeline steel, *J. Univ. Sci. Technol. Beijing*, 15(2008), No.6, p.683.

[12] H. Yu, Y. Sun, Q.X. Chen, H.T. Jiang, and L.H. Zhang, Precipitation behaviors of X70 acicular ferrite pipeline steel, *J. Univ. Sci. Technol. Beijing*, 13(2006), No.6, p.523.

[13] L.F. Zhang, Indirect methods of detecting and evaluating inclusions in steel: a review, *J. Iron Steel Res. Int.*, 13(2006), No.4, p.1.

[14] Z.Y. Liu, X.G. Li, C.W. Du, L. Lu, Y.R. Zhang, and Y.F. Cheng, Effect of inclusions on initiation of stress corrosion cracks in X70 pipeline steel in an acidic soil environment, *Corros. Sci.*, 51(2009), No.4, p.895.

[15] T.Y. Jin, Z.Y. Liu, and Y.F. Cheng, Effect of non-metallic inclusions on hydrogen-induced cracking of API5L X100 steel, *Int. J. Hydrogen Energy*, 35(2010), No.15, p.8014.

[16] H. Qiu, M. Enoki, Y. Kawaguchi, and T. Kishi, A model for the static fracture toughness of ductile structural steel, *Eng. Fract. Mech*., 70(2003), No.5, p.599.

[17] R.Z. Wang, C.I. Garcia, M. Hua, K. CHO, H.T. Zhang, and A.J. Deardo, Microstructure and precipitation behavior of Nb, Ti complex microalloyed steel produced by compact strip processing, *ISIJ Int*., 46(2006), No.9, p.1345.

[18] A.M. Zhao, Y. Wang, Y.L. Chen, D. Tang, X.T. Gao, and B.Q. Zuo, Precipitation behaviors of X80 acicular ferrite pipeline steel, *Int J. Miner. Metall. Mater.*, 18(2011), No.3, p.309.